Multiple-pulse nuclear magnetic resonance of optically pumped xenon in a low magnetic field

D. Raftery,* H. W. Long, D. Shykind,† P. J. Grandinetti,‡ and A. Pines§
Materials Sciences Division, Lawrence Berkeley Laboratory and Department of Chemistry, University of California, Berkeley, California 94720
(Received 21 June 1993; revised manuscript received 14 March 1994)

Multiple-pulse coherent averaging methods are used to increase the resolution and frequency range of optically pumped xenon NMR in nutation and point-by-point precession experiments. We observe quadrupolar splittings in ^{131}Xe spectra due to the macroscopic asymmetry of pumping cells similar to those reported previously, but with reduced demands on magnetic-field homogeneity. Cell treatment with hydrogen gas increases the quadrupolar splittings by a factor of 3 over bare Pyrex cells.

PACS number(s): 33.25.Fs, 82.65.Yh

I. INTRODUCTION

Recently there has been great interest in spin-exchange optical pumping of noble gas nuclei with alkali-metal atoms [1]. Xenon in particular, with two NMR active isotopes ^{129}Xe ($I=\frac{1}{2}$) and ^{131}Xe ($I=\frac{3}{2}$), has been studied extensively. Experiments using optical techniques [2–4] have demonstrated substantial enhancements of the xenon NMR signals from low-pressure gas samples (containing $\approx 10^{16}$ xenon atoms) which are unobservable by means of conventional NMR detection using samples with thermal spin polarization.

^{129}Xe is relatively easily polarized via spin-exchange collisions with rubidium atoms [5], due to its large exchange interaction and long relaxation times. The optical pumping of ^{129}Xe has been investigated using optical detection methods to observe the effects of the cell surface and temperature on longitudinal decay times (T_1), and to elucidate details of the spin-exchange mechanism. More recently, optically pumped ^{129}Xe has been used (with conventional high-field NMR detection) as a probe of low-surface-area materials [6], and to investigate cross polarization between ^{129}Xe and ^{13}C [7] or ^{1}H [8].

The quadrupolar isotope ^{131}Xe is more difficult to study, because it has a lower spin-exchange cross section than ^{129}Xe, resulting in a polarization rate that is much slower. Additionally, ^{131}Xe relaxation times are typically an order of magnitude shorter. Low-field optically detected ^{131}Xe NMR is particularly interesting, however, since ^{131}Xe nuclear quadrupolar interactions can be used to probe gas–surface interactions in the pumping cell. In a spherical cell, the *average* quadrupolar coupling due to xenon gas–surface interactions is zero, but, in an asymmetric cell, there remains a residual quadrupolar interaction which breaks the degeneracy of the Zeeman transitions in the NMR spectrum. Initial observations of ^{131}Xe quadrupolar splittings of this type were made by Kwon, Mark, and Volk [9]. In further investigations Wu and co-workers [10,11] have observed quadrupolar splittings on the order of 100 mHz using cells with large and well-defined asymmetry. Similar methods have been employed in observations of very long gas decays used to search for spatial anisotropies [12,13], and to investigate possible nonlinearities in quantum mechanics [14,15]. Such experiments typically rely on carefully shielded and stabilized low-magnetic fields (about 0.1 G or less) in order to prevent dephasing of the observed magnetization due to magnetic-field inhomogeneities which would obscure the small quadrupolar splittings.

In this paper we describe multiple-pulse NMR techniques capable of a variety of experiments designed to remove the effects of magnetic-field inhomogeneity. Drawing on the literature of compensated radio-frequency pulse sequences and iterative schemes (see [16] and references therein), we observe optically detected xenon NMR with high resolution without the need for the magnetic-field stabilization and shielding that characterize earlier studies. We show that such pulsed NMR techniques can narrow the linewidth by more than a factor of 20, thereby facilitating the investigation of xenon-surface interactions.

II. THEORY

In this section we present a short discussion of the optical pumping and spin relaxation of ^{129}Xe and ^{131}Xe, with attention focused on the dephasing mechanisms relevant in our experiments. The theory of ^{131}Xe quadrupolar splittings in asymmetric cells is also briefly recounted.

A. Relaxation and dephasing of xenon in rubidium cells

General theories of optical pumping, spin-exchange, and relaxation have been discussed previously in the literature [1,17]. Typically, rubidium vapor is optically

*Current address: Department of Chemistry, University of Pennsylvania, Philadelphia, PA 19104.
†Current address: Intel Corp., Hillsboro, OR 97124.
‡Current address: Department of Chemistry, Ohio State University, Columbus, OH 03210.
§To whom correspondence should be addressed.

pumped by a laser within a few milliseconds, and the spin-exchange polarization rate ($1/T_{\text{pump}}$) of xenon is given by

$$\frac{1}{T_{\text{pump}}}=\frac{\Gamma}{2}[\text{Rb}]\bar{v}\sigma_{\text{xe}}\ , \tag{1}$$

where Γ is the laser pumping rate, [Rb] is the rubidium density, $\bar{v}$ is the relative velocity of xenon and rubidium atoms, and σ_{xe} is the xenon spin-exchange cross section. The rubidium density as a function of temperature T is given by the empirical formula: $[\text{Rb}]=10^{(23.97-4132/T)}$[18] (at 65 °C, $[\text{Rb}]\approx 10^{12}$ atom/cm^3). The ratio of the pumping time to the xenon relaxation time (T_1) determines the equilibrium xenon spin polarization.

Bhaskar *et al.* [2] have investigated the rubidium density-dependent relaxation of ^{129}Xe when the pumping light is turned off, and found that the relaxation rate ($1/T_1$) may be written

$$\frac{1}{T_1}=C[\text{Rb}]+\gamma_{\text{wall}}\ , \tag{2}$$

where c is a constant, and γ_{wall} is a cell-dependent wall relaxation rate. At temperatures above 100 °C, [Rb] is large so that ^{129}Xe relaxation is caused primarily by spin-exchange collisions with rubidium, and the T_1 is about 5 min (and, in the gas phase, $T_2=T_1$). Below about 60 °C, where γ_{wall} dominates, collisions with the glass walls, which contain paramagnetic impurities, cause relaxation. Nevertheless, T_1 can approach 30 min or more in coated cells.

In contrast to the case of ^{129}Xe, the T_1 for ^{131}Xe becomes short at low temperatures due to quadrupolar relaxation, as xenon atoms spend more time on the surface, the residence time being proportional to $\exp(-E/kT)$, where E is the heat of adsorption. Spin-exchange collisions with rubidium do not affect the relaxation rate until one goes to higher temperatures, where the roughly exponential increase of rubidium density also shortens the T_1. Thus there is a minimum in the relaxation rate ($1/T_1$) described by the following equation:

$$\frac{1}{T_1}=C[\text{Rb}]+\gamma e^{-E/kT}+(T_1')^{-1}\ , \tag{3}$$

where C is a constant related to the Rb-Xe spin-exchange cross section, γ is the wall-induced relaxation rate (that is now written with an explicit temperature dependence), and T_1' represents all other contributions to the spin-lattice relaxation time which are assumed to be only weakly temperature dependent [19].

Quadrupolar dephasing of nuclei due to surface collisions was discussed by Cohen-Tannoudji [20] in his studies of Hg relaxation. He assumed that the correlation time (τ_c) for the fluctuating electric-field gradient that causes quadrupolar relaxation was long compared to the sticking time, allowing the overall damping rate to be expressed as

$$T_Q^{-1}=\frac{\tau_c\tau_s}{\tau_s+\tau_v}\overline{[e^2qQ]^2}\ . \tag{4}$$

$\tau_v=V/4S\nu$ is the time between surface collisions and is inversely related to the surface-to-volume ratio and the atomic velocity ν. The ratio of the surface sticking time to the total time, $\tau_s/(\tau_s+\tau_v)$, is the probability of finding the xenon at the wall. Quadrupolar dephasing was not removed by any of the pulse sequences discussed in this paper, although it is theoretically possible to do so with a sequence of 90° pulses.

The main dephasing mechanism for both isotopes in most of our experiments was magnetic-field inhomogeneity. The B_0 homogeneity was approximately 40 ppm, resulting in a ^{129}Xe linewidth of 3 Hz, which makes it difficult to measure the small (subhertz) quadrupolar splittings in ^{131}Xe. Hahn spin echoes [21] make it possible to refocus the dephasing of the spins in an inhomogeneous field, but in the presence of gas-phase diffusion, characterized by a diffusion constant D, dephasing of transverse magnetization (M_{trans}) can still occur rapidly:

$$M_{\text{trans}}(t)=M_0e^{-2t/T_2}e^{-(2/3)\gamma_n^2(\delta B_z)^2Dt^3}\ . \tag{5}$$

In this equation γ_n is the gyromagnetic ratio of the nucleus. In the nutation experiments (where the radio-frequency field is applied continuously) it is the inhomogeneity of the radio-frequency field that limits the resolution, particularly for the larger cells studied. Such inhomogeneity can largely be alleviated by means of coherent averaging and iterative pulse sequences, originally designed to increase the tolerance and selectivity of multiple-pulse and spin-decoupling schemes.

B. Surface-induced quadrupolar energy splittings

The spin Hamiltonian for ^{131}Xe atoms in the pumping cells consists of two parts:

$$H=-\hbar\gamma H_0I_z+H_Q\ . \tag{6}$$

$\gamma H_0=\omega_0$ is the Larmor frequency for xenon in the gas phase, that is about 17 kHz in our 49-G field, and H_Q is the quadrupolar term arising from the interaction of the quadrupolar ^{131}Xe nucleus with the electric-field gradients at the surface of the optical pumping cells. Induced distortions of the electron shells can enhance the electric-field gradients experienced by the nucleus (the Sternheimer antishielding effect [22,23]). For ^{131}Xe the gradients are enhanced by a factor of 138 [24,25], which accounts for the high sensitivity of xenon to the field gradients. In the optical-pumping experiments, the electric field gradient is assumed to be axially symmetric ($\eta=0$) with the axis perpendicular to the surface. Due to the short adsorption time of the xenon at the surface, the time-averaged quadrupolar interaction is small, so that $H_Q\ll H_Z$, and to first order we can consider only the secular part of the quadrupolar Hamiltonian in the laboratory frame:

$$H_Q=\frac{e^2qQ}{4I(2I-1)}(3I_z^2-I^2)\tfrac{1}{2}(3\cos^2\theta-1)\ . \tag{7}$$

The angular part of Eq. (7) must be averaged over the particular cell geometry used, and weighted by the fraction of time spent on the surface. For very thin cylindri-

cal cells the average quadrupole interaction is inversely proportional to the cell height, and the NMR spectrum has a central transition at ω_0 plus two satellites at $\omega_0 \pm \omega_Q$.

In a nutation experiment, the signal is observed at the nutation frequency ω_1, and the new Hamiltonian is obtained by transforming Eq. (7) to the rotating frame [22,26]. The result is that the quadrupolar interaction is modified by a factor $(3\cos^2\beta - 1)/2$, where β is the angle between the axis of nutation and the laboratory z axis. For the on-resonance case, which was used exclusively, $\beta = \pi/2$, and the splitting between the satellite transitions is scaled by a factor of $\frac{1}{2}$.

III. EXPERIMENT

Because of the sensitivity of xenon spectra to cell preparation, we describe the construction procedure for our cells in detail. The optical-pumping and detection apparatus is described and the experimental procedure outlined.

A. Cell preparation

Cylindrical cells are constructed using circular Pyrex plates 2 mm thick and 50 mm in diameter, sealed onto the ends of a cylindrical tube. A small glass tube on the side of the cylinder is connected to a stopcock with a $\frac{1}{4}$-in. connection to a gas rack. The cells are washed with distilled water and acetone and dried overnight at 90 °C in air. In the case of coated cells, such as those used for the ^{129}Xe experiments, the cells are rinsed with cyclohexane, then washed three times with a 10% solution of Surfrasil (Pierce Chemical Co., Rockford, IL) in cyclohexane, and finally cleaned with pure cyclohexane to eliminate any unreacted Surfrasil.

The cells are then evacuated at 10^{-5} torr at 120 °C overnight. Rubidium metal is placed in the bottom of the stopcock tube in a nitrogen- or argon-filled glovebox, and the tube is remounted on the gas rack. A small amount of the rubidium is distilled over to the cell using a gas torch. Cells are filled with a few torr of enriched ^{129}Xe (80%, Isotec Inc.) or ^{131}Xe (70%, EG&G Mound) which is then frozen onto the bottom of the stopcock tube, during which time either pure nitrogen or 8% hydrogen in nitrogen buffer gas is added. After waiting for the gases to mix [5], the cells are carefully torched off and cured at 120–150 °C for a week or more. The curing process has been shown to be important in ^{131}Xe cells [11], and we often failed to observe quadrupolar splittings, or even rubidium absorption, in uncured cells or cells cured for a week at only 70 °C.

B. Apparatus

A schematic drawing of the experimental apparatus is shown in Fig. 1. The glass sample cells are held in a Plexiglas oven that is heated using hot, flowing nitrogen gas, and feedback controlled to better than 0.1 °C. A large solenoid magnet of an overwound design [27], 100 cm long and 30 cm in diameter, produces a field of about 49 G when driven by a home-built 5-A constant-current power supply with 10 ppm/°C stability. The field homogeneity is corrected by observing the transient NMR signal from a water sample using standard pulsed NMR detection circuitry at 209 kHz. The corrections are made with four coils (X, Y, Z, Z^2) mounted within the magnet, and result in a homogeneity of better than 40 ppm over a 100-cm^3 sample volume.

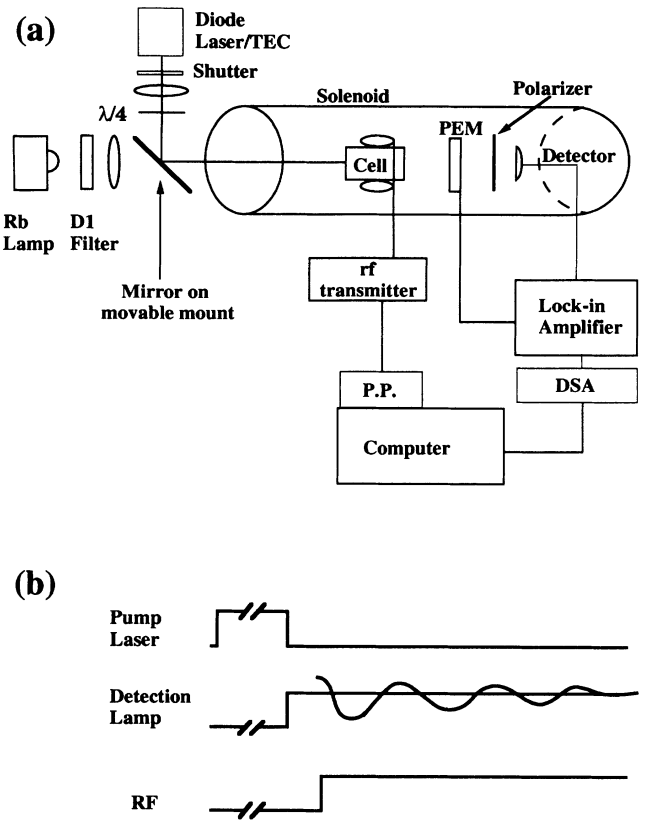

FIG. 1. (a) Schematic diagram of the experimental apparatus as described in the text. P.P. is the pulse programmer, DSA is the digital signal averager. TEC denotes a thermoelectric cooler, and PEM is a photoelastic modulator. Shim coils and oven are not shown. (b) Timing diagram for a typical experiment.

Radio-frequency pulses are applied to the sample using a transmitter controlled by a home-built pulse programmer card in an IBM compatible computer. The pulse programmer consists of $1k \times 32$ bits of first-in-first-out (FIFO) memory that contains timing and digital word information which is clocked out using an on-board 1-MHz oscillator. The pulse programmer controls all timing of events in the experiment including opening and closing rf gates, moving the mirror, and triggering the data acquisition. Frequencies of up to 1 MHz are derived from an external frequency synthesizer, and can be gated by the pulse programmer to create rf pulses. A phase shifter produces 0, 90, 180-, and 270-degree phase-shifted rf pulses using digital flip-flops. The pulses are then filtered, amplified, and sent to the tuner rf circuit. Several typical experimental pulse sequences are illustrated in Fig. 2, and discussed in detail in Sec. IV.

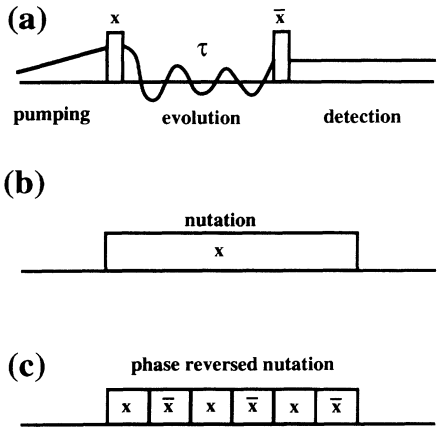

FIG. 2. Pulse schemes used in the various experiments. (a) The point-by-point experiments consist of two $\pi/2$ pulses separated by the desired evolution time τ (during which other pulses may be applied). The nutation experiments consist of either (b) a single long pulse, or (c) an alternating sequence of x and $\bar{x}$ pulses.

The sample cell is optically pumped using circularly polarized light from a 40-mW Sharp LT016 laser diode laser operating at 794.7 nm. The laser is contained in a vacuum enclosure that is either evacuated or filled with nitrogen to avoid water condensation. The laser wavelength is tuned to the rubidium D_1 absorption line by lowering the temperature to approximately $-38\,^{\circ}\mathrm{C}$ using thermoelectric coolers. The laser temperature can be controlled to better than $0.01\,^{\circ}\mathrm{C}$ using a thermistor and feedback current controller circuit. After pumping the sample for typically two minutes, a shutter blocks the laser, the mirror is moved using a stepper motor, and the cell is irradiated with unpolarized light from a Rb discharge lamp (based on a design by Brewer [28]). The unpolarized light probes the birefringence induced in the rubidium vapor by the polarized xenon system. The polarized portion of the detection light is modulated using a photoelastic modulator (model PEM080 Hinds Internationsl Inc.), analyzed with a linear polarizer, and detected by a silicon photodetector. The signal, proportional to the xenon polarization, is fed into a lock-in amplifier (Stanford Research 575) whose time constant determines the bandwidth of the experiment, and then digitized using an 8-bit Textronix DSA602 digital oscilloscope. Up to 25 accumulations are typically made in order to improve the signal-to-noise ratio in the nutation experiments. Offsets due to slow drifts are reduced by reading in and compensating for the dc value of the polarization from the lock-in system before acquisition.

To perform the T_1 measurements on ^{131}Xe, the lock-in is set to a long-time constant (1–3 sec) and the decay of $\langle I_z \rangle$ probed after pumping. When necessary, the background signal from ^{129}Xe is reduced by applying a gradient rf field at the ^{129}Xe resonance frequency (57 kHz) during the pumping period. In addition, the signal is acquired using a two-step phase cycle in which the odd acquisitions are shifted in phase by 180° while the ^{131}Xe magnetization is inverted with a rf pulse prior to acquisition. In this manner, the ^{131}Xe signals are added while the background signals and long-term drift tend to cancel upon successive runs.

IV. RESULTS AND DISCUSSION

A pointwise acquisition scheme used for ^{129}Xe is described, and the results of some typical experiments presented. This technique allows standard NMR pulse experiments to be performed on our apparatus which can only detect the xenon longitudinal magnetization. Compensated nutation sequences are discussed for ^{129}Xe and ^{131}Xe, with emphasis on the results from thin cells. Finally T_1 measurements for ^{131}Xe are mentioned.

A. Point-by-point experiments

Point-by-point acquisition is important in many areas of magnetic resonance including two-dimensional NMR [29], zero-field NMR [30,31], optically detected electron-spin resonance (ESR) [32], and the detection of multiple quantum coherences [33]. In our experiments the evolution of the system under Zeeman and quadrupolar interactions in the transverse plane occurs during the time between two $(\pi/2)$ rf pulses that initiate and terminate evolution. The evolution time is incremented between successive pump and acquisition cycles of the experiment, allowing the time development of the magnetization to be mapped out. In Fig. 2(a), the evolution is initiated by a $(\pi/2)_x$ pulse which converts the z magnetization (enhanced by optical pumping in our case) to x magnetization in the transverse plane. Evolution is later terminated by a $(\pi/2)_{\bar{x}}$ pulse reconverting the x component of the magnetization in the rotating frame back into z magnetization that can be monitored using optical detection. A $(\pi/2)_y$ pulse can be used to recover the quadrature component of the magnetization in the rotating frame, although this was not necessary in the current experiments. Optical detection of the z magnetization is particularly sensitive because the only time evolution arises from the very slow T_1 relaxation (minutes), allowing extended lock-in time constants.

Figure 3 shows the results from several experiments. The first result [Fig. 3(a)] is a free-induction decay (FID) of ^{129}Xe that shows a decay time of about 0.3 sec, caused by the inhomogeneities in the magnetic field (δB_0) not averaged by gaseous diffusion inside the pumping cell. The second result [Fig. 3(b)] demonstrates a CPMG (Carr-Purcell-Meiboom-Gill) sequence [34], which is designed to refocus dephasing such as that caused by δB_0. In this case the decay time extrapolates to approximately 3 sec, the limitation being due to pulse imperfections and diffusion in the period between the 180° pulses. We have also performed spin-locking experiments [Fig. 3(c)] with this technique (which yielded slightly longer decay times than the CPMG sequences), as well as spin-echo experiments which can be used to measure diffusion constants.

These experiments were not optimal for ^{131}Xe, however, because of the limited signal-to-noise ratio resulting from the inferior spin-exchange rate and shorter T_1 com-

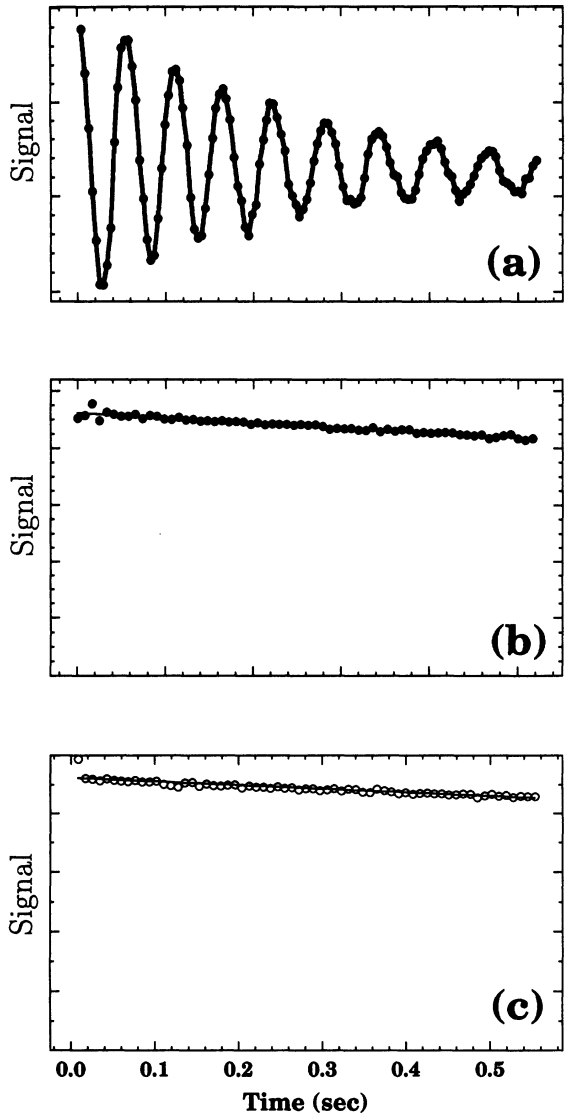

FIG. 3. Point-by-point acquisition of optically pumped and optically detected ^{129}Xe signal. (a) Free-induction decay, decay time =0.3 sec. (b) CPMG sequence (see text), decay time =3 sec. (c) Spin-locking experiment, decay time =8 sec.

pared to ^{129}Xe [9], as well as our limited laser power (40 mW). It should be noted that the nutation experiments (discussed below) that have been used to detect the quadrupolar splittings of ^{131}Xe scale this interaction by a factor of $\frac{1}{2}$ on resonance. With point-by-point techniques it should be possible to observe the full quadrupolar splittings with no scaling, no resonance offset effects, and no magnetic shielding, assuming the signal-to-noise ratio is otherwise sufficient.

B. ^{129}Xe nutation experiments

Another way to overcome dephasing due to dc field inhomogeneities involves a nutation experiment [Fig. 2(b)] with a B_1 (rf) field much stronger than δB_0. This technique, in which the evolution of the xenon magnetization is followed directly by optical detection during the pulses, leads to a longer decay ($T_2 \approx 1.5$ sec) as shown in Fig. 4(a). The smaller dephasing effects are due to the rf field inhomogeneities δB_1. Such rf inhomogeneities can be removed using rotational echoes, i.e., by reversing the phase of the B_1 field every nutation cycle, or every 2π rotation of the xenon magnetization. In principle this can remove the dephasing entirely with rapid enough phase reversals, but the enhanced resolution comes at the expense of the signal-to-noise ratio since the lock-in amplifier time constant must be set such that

$$\omega_1 \ll \frac{1}{\tau_{\text{lock in}}} . \tag{8}$$

Figure 4(b) shows the large improvement one can achieve using the phase-reversed nutation sequence [Fig. 2(c)], with a nutation rate of 4 Hz. The decay time increases to approximately 15 sec and is now dominated by pulse imperfections and residual rf field inhomogeneities not averaged on the time scale of the nutation. We were able to perform nutation experiments on ^{131}Xe (in symmetrical cells) that decayed at essentially the $T_1/2$ limit of 50 sec. Since the rf coils were only being used for excitation there were no size constraints involving detection, and we experimented with using optimum geometry saddle coils that had a diameter of 25 cm. Even with

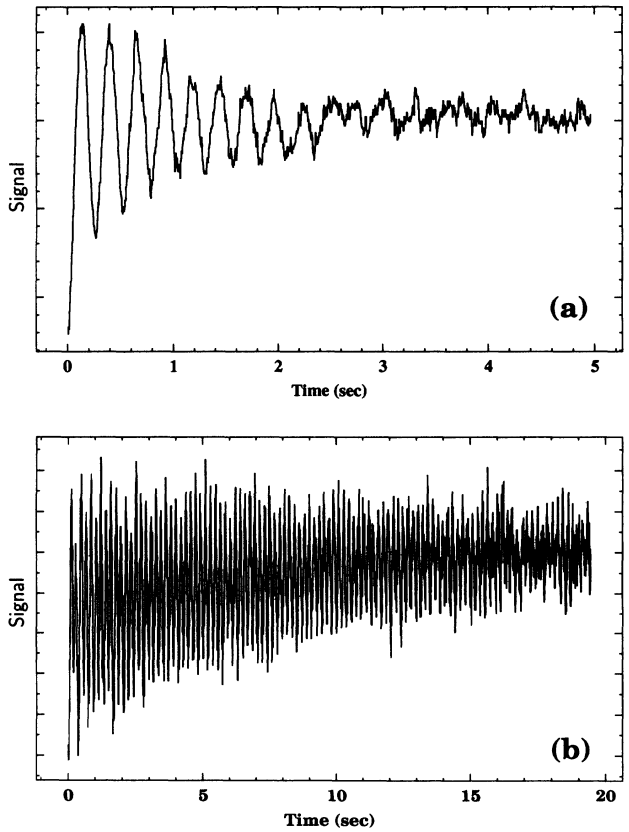

FIG. 4. Optically pumped and optically detected ^{129}Xe nutation experiment. (a) The signal rapidly decays due to magnetic-field inhomogeneities. (b) Reversing the rf nutation phase every 360° refocuses the magnetization and increases the decay time. Notice the different time scales for (a) and (b).

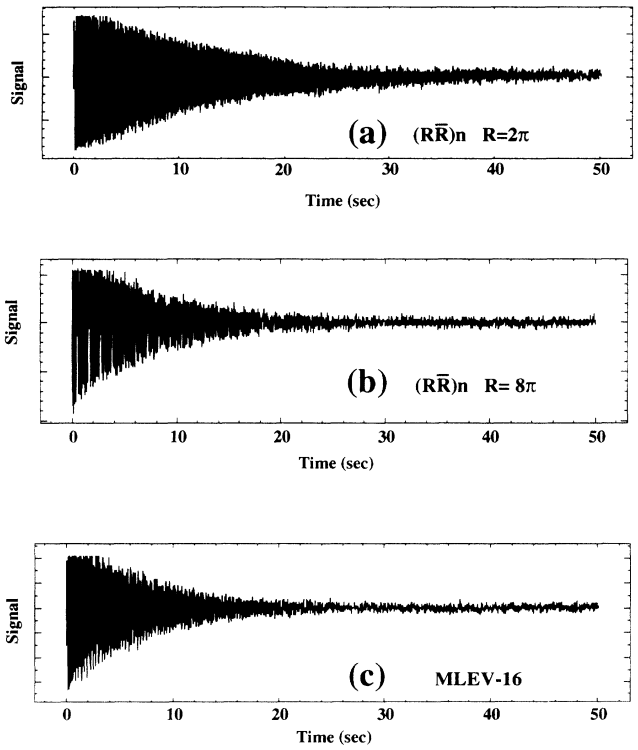

FIG. 5. Results for ^{129}Xe nutation using three different pulse schemes. Nutation sequences (described in the text) are indicated, where R represents a rotation of the magnetization by 2π or 8π.

these very large (and therefore very homogeneous) coils we found that it was still advantageous to use the phase-reversal technique to produce the longest decay.

We experimented with shorter and longer nutation periods [Figs. 5(a) and 5(b)], but found 360° to be optimal. The spectra become more complicated for cycles that are not multiples of 180° due to high-frequency harmonics introduced by suddenly changing the sign of $\langle I_z \rangle$. Higher-order corrections to the simple phase-reversed nutation pulse sequence of Fig. 2(c) can be made by using iterative NMR schemes. For example, the MLEV-16 sequence [35] is an example of an iterated sequence of rotations, R, and phase-reversed rotations, $\bar{R}$, in the following "supercycle:"

$$RR\bar{R}\bar{R}\ \bar{R}RR\bar{R}\ \bar{R}\bar{R}RR\ R\bar{R}\bar{R}R\ . \tag{9}$$

Data from ^{129}Xe experiments with a nutation frequency of about 8 Hz using $R=2\pi$ and 8π rotations, and a MLEV-16 sequence are shown in Fig. 5. The more complex sequences are designed to be insensitive to a wide bandwidth of pulse imperfections, but in our experiments they produced no improvement over simple phase alternation.

C. ^{131}Xe nutation experiments

Figure 6 shows the phase-reversed nutation data at 120 °C for ^{131}Xe in a flat cylindrical cell 3 mm high with added hydrogen. The Fourier transform shows three peaks corresponding to the three frequencies of the

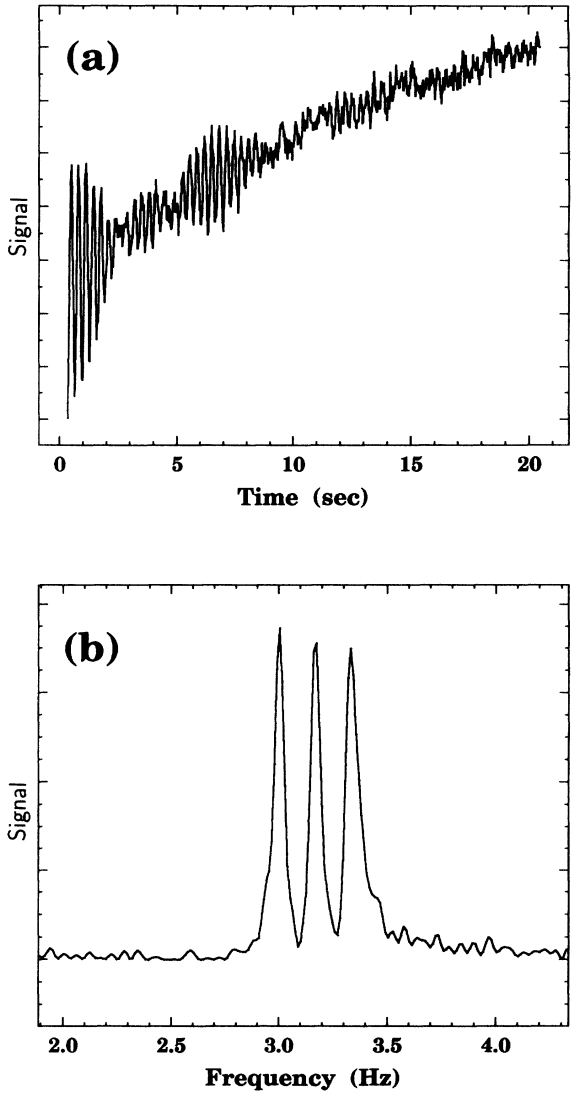

FIG. 6. (a) ^{131}Xe nutation signal for xenon in a hydrogen coated cell (3-mm height and 50-mm diameter) at 115 °C. The slow background decay arises from ^{129}Xe relaxation. (b) Fourier transform of (a) showing quadrupolar splitting of 392 mHz.

quadrupole-perturbed Zeeman Hamiltonian [Eq. (6)]. The measured quadrupolar splitting for the hydrogen cell is about three times larger than our results for a bare Pyrex cell (with no added hydrogen) under the same experimental conditions. For bare Pyrex cells the splittings had the predicted inverse dependence on cell height [10]. Splittings comparable to the hydrogen cell were detected in a quartz cell with the same dimensions after extensive curing (months), but the signal-to-noise was very poor.

Quadrupolar splittings of the bare Pyrex cell and cells with added hydrogen were measured at different temperatures, and the data fit to an Arrhenius equation

$$\omega_Q = \omega_{0Q} e^{-E/kT}\ . \tag{10}$$

The activation energies E are -0.003 eV for the bare cell, and -0.12 eV for the hydrogen cell, in agreement with results of other workers [9,11]. The higher activa-

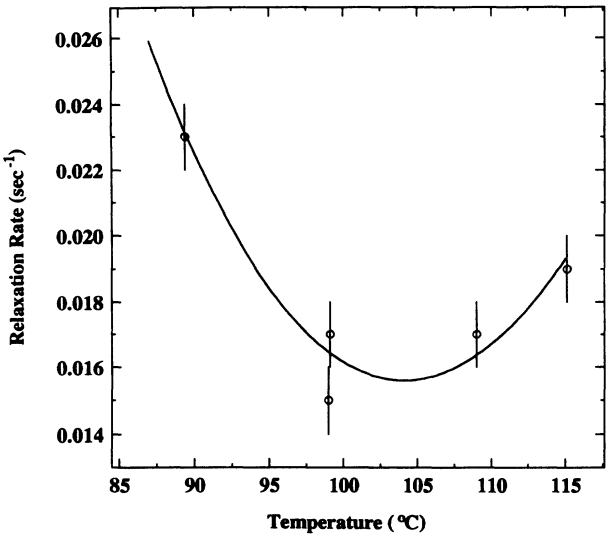

FIG. 7. T_1 data for ^{131}Xe in a hydrogen-coated cell as a function of temperature. The solid line is a fit using Eq. (3) of the text.

tion energy implies a longer residence time on the surface, which leads to the larger quadrupolar interaction for the hydrogen cells.

For the thin ($\sim$3 mm) cells, no substantial decrease in linewidth was observed as a result of the phase-reversed nutation experiments. This indicates that xenon sufficiently samples the surface and volume of the cell during the approximately 250-ms nutation time, and that the rf field was homogeneous over the cell region. In the larger cells, however, substantial narrowing was observed, as shown in Fig. 4.

D. T_1 measurements

Several researchers have reported [9,11,36] that H_2 has the effect of lengthening the T_1 of ^{131}Xe in Pyrex glass cells. This probably results from reactions of H_2 with paramagnetic centers (M) on the surface of the glass, including rubidium, to form M-H reducing the paramagnetic relaxation of xenon at the surface. Nicol [37] reported an increase in the relaxation time for ^{129}Xe in Pyrex cells by adding H_2, although the relaxation time *decreased* in Corning 1720 cells [36]. For ^{129}Xe optical-pumping experiments, the largest effect is obtained by coating the cells with Surfrasil which is also thought to react at paramagnetic sites because it has the effect of substantially lengthening the relaxation time.

The ^{131}Xe T_1 data for the hydrogen cell is shown in Fig. 7, and has the temperature dependence predicted by Eq. (3) and reported by other workers [19,38]. The values for γ (2.1×10^{-9} sec^{-1}) and $1/T_1'$ (1.1×10^{-2} sec^{-1}) derived from the fit of Eq. (3) to the data are in accordance with those reported for cells with N_2 buffer gas [19]. We were unable to obtain any spectra from ^{131}Xe in a surfrasil coated cell due to the dramatic reduction in T_1 (<10 sec [11]).

V. CONCLUSIONS

We have described a variety of multiple-pulse experimental schemes that remove the effects of magnetic-field inhomogeneities on low-field optical-pumping experiments. Point-by-point acquisition methods make it possible to implement a wide variety of NMR pulse sequences and allow the bandwidths of the evolution and observation times to be different. Phase-reversed nutation experiments yield much greater resolution than straight nutation experiments. These techniques allow accurate determination of ^{131}Xe quadrupolar interactions at the cell surface; more chemically interesting surfaces may also be investigated with ^{131}Xe and should benefit from these techniques.

ACKNOWLEDGMENTS

The authors would like to thank the chemistry department glass shop for their expert assistance in the construction of the cells used in these experiments, and C. Hawley (University of Illinois) for kindly providing the circuit diagram for the pulse programmer. This work was supported by the Director, Office of Energy Research, Office of Basic Energy Sciences, Materials Sciences Division, U.S. Department of Energy under Contract No. DE-AC03-76SF00098.

[1] R. J. Knize, Z. Wu, and W. Happer, in Adv. At. Mol. Phys. **24**, 223 (1988).
[2] N. D. Bhaskar, W. Happer, M. Larsson, and X. Xeng, Phys. Rev. Lett. **50**, 105 (1983).
[3] X. Zeng *et al.*, Chem. Phys. Lett. **182**, 538 (1991).
[4] D. Raftery *et al.*, Phys. Rev. Lett. **66**, 584 (1991).
[5] X. Zeng *et al.*, Phys. Rev. A **31**, 260 (1985).
[6] D. Raftery *et al.*, J. Phys. Chem. **97**, 1649 (1993).
[7] C. R. Bowers, H. W. Long, T. Pietrass, H. C. Gaede, and A. Pines, Chem. Phys. Lett. **205**, 168 (1993).
[8] H. W. Long *et al.*, J. Am. Chem. Soc. **115**, 8491 (1993).
[9] T. M. Kwon, J. G. Mark, and C. H. Volk, Phys. Rev. A **24**, 1894 (1981).
[10] Z. Wu, W. Happer, and J. Daniels, Phys. Rev. Lett. **59**, 1480 (1987).
[11] Z. Wu, W. Happer, M. Kitano, and J. Daniels, Phys. Rev. A **42**, 2774 (1990).
[12] S. K. Lamoreaux, J. P. Jacobs, B. R. Heckel, F. J. Raab, and E. N. Fortson, Phys. Rev. A **39**, 1082 (1989).
[13] T. E. Chupp *et al.*, Phys. Rev. Lett. **63**, 1541 (1989).
[14] T. E. Chupp and R. J. Hoare, Phys. Rev. Lett. **64**, 2261 (1990).

[15] P. K. Majumder, B. J. Venema, S. K. Lamereaux, B. R. Heckel, and E. N. Fortson, Phys. Rev. Lett. **65**, 2931 (1990).
[16] A. J. Shaka and J. Keeler, Prog. NMR Spec. **19**, 47 (1987).
[17] W. Happer, Rev. Mod. Phys. **44**, 169 (1972).
[18] T. Killian, Phys. Rev. **27**, 578 (1926).
[19] C. H. Volk, T. M. Kwon, J. G. Mark, Y. B. Kim, and J. C. Woo, Phys. Rev. Lett. **44**, 136 (1980).
[20] C. Cohen-Tannoudji, J. Phys. **24**, 653 (1963).
[21] E. L. Hahn, Phys. Rev. **80**, 580 (1950).
[22] C. P. Slichter, *Principles of Magnetic Resonance* (Springer, Berlin, 1990).
[23] R. M. Sternheimer, Phys. Rev. **105**, 158 (1957).
[24] P. Ingman, J. Jokasaari, and P. Diehl, J. Magn. Res. **92**, 163 (1991).
[25] M. R. Keenan, L. W. Buxton, E. J. Cambell, T. J. Balle, and W. Flygare, J. Chem. Phys. **73**, 3523 (1980).
[26] M. Mehring, *Principles of High Resolution NMR in Solids* (Springer, Berlin, 1983).
[27] M. W. Garrett, J. Appl. Phys. **38**, 2563 (1967).
[28] R. G. Brewer, Rev. Sci. Instrum. **32**, 1356 (1961).
[29] R. R. Ernst, G. Bodenhausen, and A. Wokaun, *Principles of Nuclear Magnetic Resonance in One and Two Dimensions* (Clarendon, Oxford, 1987).
[30] D. P. Weitekamp, A. Bielecki, D. Zax, K. Zilm, and A. Pines, Phys. Rev. Lett. **50**, 1807 (1983).
[31] D. B. Zax, A. Bielecki, K. W. Zilm, A. Pines, and D. P. Weitekamp, J. Chem. Phys. **83**, 4877 (1985).
[32] W. G. Breiland, C. B. Harris, and A. Pines, Phys. Rev. Lett. **30**, 158 (1973).
[33] L. Emsley and A. Pines, in *Nuclear Magnetic Double Resonance, Proceedings of the CXXIII School of Physics "Enrico Fermi,"* edited by B. Maraviglia (North-Holland, Amsterdam, 1993), pp. 123–258.
[34] S. Meiboom and D. Gill, Rev. Sci. Instrum. **29**, 6881 (1958).
[35] M. H. Levitt, R. Freeman, and T. Frenkiel, J. Magn. Res. **50**, 157 (1982).
[36] A. T. Nicol, U.S. Air Force Technical Report AFOSR-TR-82-0418 (1982) (unpublished).
[37] A. T. Nicol, Phys. Rev. B **29**, 2397 (1984).
[38] Z. Liu, X. Sun, X. Zeng, and Q. He, Chin. Phys. Lett. **7**, 399 (1990).

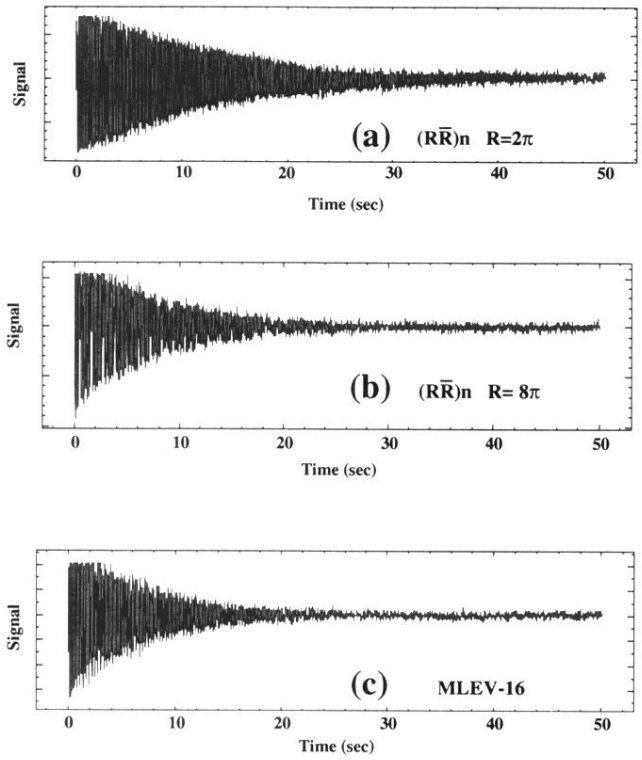

FIG. 5. Results for ^{129}Xe nutation using three different pulse schemes. Nutation sequences (described in the text) are indicated, where R represents a rotation of the magnetization by 2π or 8π.